Original Article

MOLECULAR METABOLISM

Unique pharmacology of a novel allosteric agonist/sensitizer insulin receptor monoclonal antibody

Simon A. Hinke [1,*], Anne M. Cieniewicz [2], Thomas Kirchner [1], Katharine D'Aquino [1], Rupesh Nanjunda [2], Jason Aligo [2], Robert Perkinson [2,3], Philip Cooper [2], Ken Boayke [2], Mark L. Chiu [2], Steve Jarantow [2], Eilyn R. Lacy [2], Yin Liang [1], Dana L. Johnson [1], Jean M. Whaley [1], Russell B. Lingham [2], Anthony J. Kihm [2,]**

ABSTRACT

Objective: Insulin resistance is a key feature of Type 2 Diabetes (T2D), and improving insulin sensitivity is important for disease management. Allosteric modulation of the insulin receptor (IR) with monoclonal antibodies (mAbs) can enhance insulin sensitivity and restore glycemic control in animal models of T2D.

Methods: A novel human mAb, IRAB-A, was identified by phage screening using competition binding and surface plasmon resonance assays with the IR extracellular domain. Cell based assays demonstrated agonist and sensitizer effects of IRAB-A on IR and Akt phosphorylation, as well as glucose uptake. Lean and diet-induced obese mice were used to characterize single-dose in vivo pharmacological effects of IRAB-A; multiple-dose IRAB-A effects were tested in obese mice.

Results: *In vitro* studies indicate that IRAB-A exhibits sensitizer and agonist properties distinct from insulin on the IR and is translated to downstream signaling and function; IRAB-A bound specifically and allosterically to the IR and stabilized insulin binding. A single dose of IRAB-A given to lean mice rapidly reduced fed blood glucose for approximately 2 weeks, with concomitant reduced insulin levels suggesting improved insulin sensitivity. Phosphorylated IR (pIR) from skeletal muscle and liver were increased by IRAB-A; however, phosphorylated Akt (pAkt) levels were only elevated in skeletal muscle and not liver vs. control; immunochemistry analysis (IHC) confirmed the long-lived persistence of IRAB-A in skeletal muscle and liver. Studies in diet-induced obese (DIO) mice with IRAB-A reduced fed blood glucose and insulinemia yet impaired glucose tolerance and led to protracted insulinemia during a meal challenge.

Conclusion: Collectively, the data suggest IRAB-A acts allosterically on the insulin receptor acting non-competitively with insulin to both activate the receptor and enhance insulin signaling. While IRAB-A produced a decrease in blood glucose in lean mice, the data in DIO mice indicated an exacerbation of insulin resistance; these data were unexpected and suggested the interplay of complex unknown pharmacology. Taken together, this work suggests that IRAB-A may be an important tool to explore insulin receptor signaling and pharmacology.

Keywords Insulin; Insulin receptor; Positive allosteric modulator; Monoclonal antibody; Diabetes

1. INTRODUCTION

A ubiquitous feature of T2D is decreased sensitivity to insulin [1]. In addition to insulin restoring some glycemic control and preventing diabetes-related complications [1], insulin sensitizers such as thiazolidinediones [2,3] can impact insulin resistance yet have been associated with weight gain and cardiac events [4–6]. There is a need for novel, insulin-sensitizing agents that are devoid of side-effects that may provide safer and more effective means to treat T2D.

We sought to identify novel insulin sensitizers by screening human phage monoclonal antibody (mAb) libraries to identify mAbs that could bind orthosterically or allosterically to the IR and act as positive allosteric regulators [7]. Several reports have described endogenous agonist and/or antagonist IR auto-antibodies [8–13] and IR allosteric

[1]Cardiovascular and Metabolism Therapeutic Area, Janssen Pharmaceutical Research & Development LLC, 1400 McKean Road, Spring House, PA, 19477, USA [2]Janssen BioTherapeutics, Janssen Pharmaceutical Research & Development LLC, 1400 McKean Road, Spring House PA 19477, USA

[3] Current affiliation: Glaxo Smith Kline, 1250 South Collegeville Road, Collegeville, PA, 19426, USA.

*Corresponding author. E-mail: shinke@its.jnj.com (S.A. Hinke).

**Corresponding author. E-mail: AKihm3@its.jnj.com (A.J. Kihm).

Abbreviations: T2D, Type 2 Diabetes Mellitus; IR, insulin receptor; Akt, protein kinase B; mAb, monoclonal antibody; DIO, diet-induced obesity; HFD, high fat diet; Fab, antigen binding antibody fragment; Abs, antibodies; ECD, extracellular domain; ELISA, enzyme-linked immunosorbent assay; SPR, surface plasmon resonance; PBS, phosphate buffered saline; BSA, bovine serum albumin; KRPH, Kreb's ringer phosphate HEPES buffer; MMTT, mixed meal tolerance test; OGTT, oral glucose tolerance test; STZ, streptozotocin

Received October 6, 2017 • Revision received January 2, 2018 • Accepted January 17, 2018 • Available online 3 February 2018

https://doi.org/10.1016/j.molmet.2018.01.014

mAbs that are agonists, insulin sensitizers, or antagonists derived from targeted screens [7,14]. Our screening approach has previously identified IRAB-B, an allosteric antagonist of IR [14]. Collectively, the available data provide evidence that the insulin receptor can be engaged with antibodies to influence insulin signaling and that one or more mAbs may ultimately be developed into a therapeutic to regulate T2DM and/or provide tools to understand insulin signaling.

In this report, we characterize a novel mAb, IRAB-A. *In vitro* testing with IRAB-A indicates that it binds allosterically to the IR, reduces the off-rate of insulin from the IR, and influences IR signaling demonstrating both sensitizer and agonist properties distinct from those of insulin. In lean mice, IRAB-A reduced glucose and insulin levels, while in DIO mice, IRAB-A decreased ambient glycemia and insulin, but following a meal challenge led to unexpected hyperglycemia. Taken together, the results demonstrate the unique pharmacology of a novel IR antibody that can impact insulin signaling and glucose control. This mAb can also be used to better evaluate IR biology and insulin physiology to better guide therapeutic strategies for managing insulin resistance and T2D.

2. METHODS

2.1. Identification of anti-insulin receptor antibodies

Antigen-binding fragment (Fab) phage display panning was conducted to identify insulin receptor binding antibodies (Abs). The long isoform of the human IR extracellular domain (ECD) (Met1-Lys956; Sino Biologicals) was biotinylated and used as an antigen for panning with a panel of human Fab libraries. After three rounds of panning, binding was confirmed by ELISA screen, and successful binders were expressed as human Abs (hIgG1). Also, some constructs were created by grafting the cDNA sequences of the variable region of the IRAB-A on cDNA of a mouse IgG2σ cDNA construct that were then expressed and purified as mAbs. Monomeric Abs were screened against HuH7 cells with and without the presence of human insulin (Sigma). Abs that bound to cells were then evaluated in a competitive binding via MSD assay and sorted into different epitope bins [14].

2.2. Binding affinity studies by surface plasmon resonance (SPR)

IRAB-A binding to recombinant IR constructs (short or long isoforms) and insulin binding to IR/IRAB-A complex were tested by ProteOn SPR using protocols reported elsewhere [14]. To test the binding of insulin to IR in the absence of IRAB-A, the poly-histidine tagged recombinant IR constructs were captured on a HTG sensor chip through Tris-NTA surface chemistry. Serial dilutions of insulin (400 nM – 1.56 nM at 4-fold dilutions) were prepared in phosphate buffered saline (PBS with 0.005% P20; BioRad) and were injected over IR captured surface to monitor binding (association and dissociation for 5 and 20 min, respectively). SPR sensorgrams were processed using ProteOn Manager software (BioRad, Hercules, CA) and affinity analyses were performed using a 1:1 Langmuir Binding model (IRAB-A binding to IR or insulin binding to IR/IRAB-A complex) and an Equilibrium Steady-State model (insulin binding to IR).

2.3. Cell culture

For IR phosphorylation assays, HuH7 cells were plated at 50,000 cells/well (100 μL) in 96-well plates in DMEM + GlutaMAX (Gibco) with 10% heat-inactivated FBS and incubated at 37 °C in 5% CO_2 for 18–24 h before use. U2OS cells (DiscoverX) were plated at 10,000 cells/well (in 20 μL using Assay Complete Cell Plating 16 Reagent and Assay Complete U2OS Cell Culture Kit 10; DiscoverX) in Costar White 384 TC treated assay plate and incubated at 37 °C in 5% CO_2 for 18–24 h before use. 3T3-L1 fibroblasts were maintained in DMEM containing 10% cosmic calf serum (HyClone) and 5% CO_2 at 37 °C. Two days after reaching confluence, differentiation was induced by incubating cells for 48 h in DMEM containing 10% FBS, 0.5 mM isobutylmethylxanthine (IBMX; Sigma), 0.25 mM dexamethasone (DXM; Sigma), and 1 μg/mL insulin (Sigma). After 2 days, the IBMX and DXM were removed, and insulin was maintained for 2 additional days. After this period, insulin was removed, and cells completely differentiated. The cells were then used at 9–12 days post-differentiation.

2.4. Cell-based assays

Initial mAb hit screening was performed using a U2OS IR/beta-galactosidase complementation assay with a chemiluminescent readout (PathHunter; DiscoverRx). mAbs and Humulin were diluted in U2OS cell plating media; mAb dilutions were added for 30 min at room temperature followed by insulin stimulation for 3 h at room temp. PathHunter detection reagent was added for 1 h at room temp and read on Envision Plate Reader. For HuH7 assays, recombinant human insulin (Humulin R; Eli Lilly) and IRAB-A were diluted in culture media. All treatments were performed at 37 °C. Reactions were stopped by aspirating media and washing cells with ice-cold PBS. MSD Lysis Buffer (with protease and phosphatase inhibitors) was added. Plates were shaken for 30 min at room temperature and frozen at −80 °C until analysis.

Glucose uptake was measured in differentiated 3T3-L1 fibroblasts; cells were washed with PBS (Corning) and serum starved for 16 h in DMEM + 0.2% BSA (Sigma). Cells were washed once with PBS and once with Krebs–Ringer phosphate HEPES buffer (KRPH) (20 mM HEPES, 10 mM $NaPO_4$, 0.9 mM $MgSO_4$, 0.9 mM $CaCl_2$, 136 mM NaCl, 4.7 mM KCl [pH 7.4]) + 0.2% BSA. Cells were incubated in KRPH + 0.2% BSA for 1 h at 37 °C. Cytochalasin B 1 μM (Sigma) was added to select wells, and cells were incubated for 1 h at 37 °C. IRAB-A was added for 15 min followed by insulin for 15 min at 37 °C and then a 10 × solution of 2-deoxyglucose (Sigma) and [3H]-2-deoxyglucose (PerkinElmer) in KRPH + 0.2% BSA for a final concentration of 100 μM 2-deoxyglucose, and 0.5 μCi/mL [3H]-2-deoxyglucose was added for an additional 15 min. Cells were washed five times with ice-cold PBS and lysed with 0.05% SDS/PBS shaking for 30 min at room temperature. An aliquot of the lysate was added to Microscint-20 (PerkinElmer) scintillation fluid, and 3H was counted on the PerkinElmer TopCount NXT. Total protein was determined by Pierce BCA Protein Assay Kit (Thermo Fisher). Counts per minute were normalized to total protein and cytochalasin B control.

2.5. MSD analyses of insulin signaling

HuH7 cell lysates were thawed on ice immediately before analysis. Meso Scale Discovery (MSD) assays were performed using the Insulin Signaling Panel (Total Protein) and Insulin Signaling (Phospho Protein) kits, Phospho-Akt (Thr308) Whole Cell Lysate Kit and Phospho (Ser473)/Total Akt Whole Cell Lysate Kit. MSD plates were blocked for 1 h at room temperature in MSD blocking buffer with vigorous shaking. Cell lysates were added to appropriate wells and the plates shaken at room temperature for 1 h. Primary antibodies from Insulin Signaling Panel and Akt Signaling Kits were diluted to 1/50. Ab dilutions were added to appropriate wells and shaken at room temperature for 1 h. Plates were washed three times between each step. MSD Read Buffer was added to wells and read on an MSD Plate Reader.

2.6. Tissue preparation and immunofluorescent imaging

Tissues were collected immediately at necropsy and embedded as frozen tissue blocks via standard methods. Cryosections were

collected on microscope slides and fixed in ice cold acetone prior to immunohistochemistry staining to detect IRAB-A levels. Immunohistochemistry was performed using a Ventana Discovery Ultra automated platform (Roche Diagnostics). Tissues derived from animals dosed with an isotype control mAb (CNTO3930; [15]) were also stained alongside tissue samples from IRAB-A-treated animals. Briefly, after tissue fixation, slides were loaded onto the instrument and stained with goat anti-human IgG (H + L, Jackson Immunoresearch, West Grove, PA) to detect IRAB-A. The slides were then stained with a bovine anti-goat-HRP antibody (Roche Diagnostics). Visualization was performed using an HRP-based FITC detection system (Roche Diagnostics). The slides were then washed in water with detergent, rinsed in PBS, and coverslipped using Vectashield HardSet Antifade Mounting Medium with DAPI (Vector Labs, Burlingame, CA). All images were obtained from a Nikon Eclipse E800 fluorescent microscope (Minato, Tokyo, Japan) at 40× magnification using standard filter sets with Nikon software (Nikon Elements Advanced Research) and Adobe Photoshop (Adobe, San Jose, CA) using the same parameters for all images.

2.7. In vivo studies

All animal studies were performed with prior approval from the Janssen Institutional Animal Use and Care Committee, in accordance with NIH guide for the care and use of animals in research. Male C57Bl6/N mice were obtained from Taconic (Hudson, NY), maintained on standard 5K75 rodent diet or D12492 60% high fat diet (Research Diets, New Brunswick, NJ), with free access to drinking water. Mice were housed 1–2/cage in ventilated, temperature controlled racks, with a 12 h light/dark cycle. Studies in lean mice were performed in animals that were 6–8 weeks of age or 18–20 weeks of age. Diet induced obese C57 mice were generated by 6 or 12 weeks of high fat diet starting at 6 weeks of age. IRAB-A or controls were injected subcutaneously at a dose volume of 10 ml/kg, with the test article diluted appropriately in sterile PBS to achieve the reported doses.

Glycemia measurements were obtained from whole blood obtained from tail nicks using a handheld OneTouch Ultra Glucometer (LifeScan, Chesterbrook, PA). Oral glucose tolerance testing of lean mice was done following overnight fasting. Baseline fasting blood glucose was measured prior to a 2 g/kg gavage (20% glucose, 10 ml/kg). Blood glucose was measured at the indicated timepoints over 2 h following the glucose challenge. A mixed meal tolerance test (MMTT) was administered to DIO mice following a 6 h fast using similar methods but using Strawberry Boost Plus (Nestle) supplemented with glucose to deliver a 2 g/kg challenge.

Plasma or serum samples for hormonal analysis or antibody exposure were similarly taken from tail bleed samples into Starstedt capillary collection tubes. For plasma separation, EDTA blood samples were held on ice following collection, and centrifuged at 4 °C (10 min/10,000 rpm); serum separation was performed following 30–60 min incubation of whole blood at room temperature, prior to centrifugation. Plasma or serum samples were stored at −80 °C until analysis. Hormone measurement was performed per the manufacturer's protocols for mouse insulin (MSD), C-peptide (Alpco, Salem, NH) and glucagon (Mercodia, Uppsala, Sweden). Detection of exogenous antibody concentrations in serum was performed using a MSD electrochemiluminescent assay. Biotin-mouse anti-human Ig kappa light chain (BD Pharmingen, San Jose, CA) was used as capture antibody; pan anti-human Fc IgG1/IgG2 antibody R10Z8E9 (R10) was labeled with MSD Sulfo-TAG NHS Ester and used as detection antibody. CNTO3930 human IgG1 control was used to generate a standard curve to quantify serum levels of IRAB-A or control mAb.

Tissues were harvested for phosphoprotein analysis following cervical dislocation and snap freezing in nitrogen. Samples were homogenized on ice in Tris Lysis Buffer (MSD) containing Complete Protease Inhibitors (Roche) and PhosStop (Roche), and clarified by refrigerated centrifugation (14,000 rpm/4C/10 min). Protein concentration was measured by BCA assay (Pierce) and ELISA for phospho-Insulin Receptor beta (Tyr1150/1151) Assay (Cell Signaling) and phospho-Ser473 or phospho-Thr308-Akt Assay (MSD) performed as per manufacturer's specifications using uniform protein concentration.

In preparation for chronic dosing of DIO mice, an immunologically muted version of IRAB-A was produced on a mouse IgG2σ Fc backbone (mIRAB-A). This derivative antibody was tested in vitro and in vivo demonstrating similar behavior to the human IgG1 based IRAB-A (Supplemental Fig. S1). The pharmacokinetics of mIRAB-A supported a twice weekly dosing regimen for chronic studies. To permit comparison to acute studies on 18 wk old DIO mice, BIW dosing of DIO mice was initiated in 14 wk old mice (8 weeks on 60% HFD at start) for a 28-day chronic study. Weekly fed blood glucose and insulin samples were taken over the course of the experiment, and a 6-hour fasting mixed meal tolerance test was performed on day 24, as described previously. Terminal blood chemistry was assessed on day 30, including insulin, glucagon, HbA1c determination, and plasma lipids, along with necropsy measurements: liver, pancreas and eWAT mass, pancreatic insulin content, and liver fat content.

2.8. Statistics

Data are presented as Mean ± Standard Error of the Mean, with the number of independent replicates noted in the figure legends. Data were analyzed and graphed using GraphPad Prism (v. 7.00). T-tests or ANOVA was used, where appropriate, to establish significant differences among test groups with a cutoff of $P < 0.05$; Dunnett's multiple comparison test was used to determine differences between test groups versus the control condition.

3. RESULTS

3.1. Identification of IRAB-A and impact on receptor binding

SPR studies show that IRAB-A bound to both IR ECD constructs (A or B) with low nanomolar affinities and was driven by slow dissociation from the complex ($K_D \approx 2$–3 nM; Table 1; Figure 1A). The binding affinity of insulin alone with IR was substantially weaker with very fast dissociation ($K_D \approx 110$ nM; Figure 1B,D); steady-state analysis is shown in Figure 1F. When insulin binding affinity was re-tested following pre-treatment of IR with IRAB-A, the binding affinity of insulin for IR was increased by >50-fold ($K_D \approx 1.7$ nM) due to slowing of insulin dissociation kinetics from the IR/IRAB-A complex (Figure 1C,E). Furthermore, we performed an ELISA-based screen to determine whether IRAB-A bound with the IGF-I receptor. Results showed that binding of IRAB-A to the IGF-I receptor was equivalent to that of background controls (data not shown).

3.2. IRAB-A alters IR signaling and increases receptor sensitivity to insulin in vitro

The impact of IRAB-A on IR signaling was evaluated in a U2OS reporter cell line engineered to over-express the long receptor isoform (IR-B). Insulin dose titration experiments were performed in the presence of increasing concentrations of IRAB-A or isotype control antibody (Figure 2A,B). IRAB-A induces a leftward-shift of the insulin dose response curve (decreased EC_{50}) as well increasing the overall response to insulin (C_{max}) while the isotype was without effect. In

Table 1 — Surface Plasmon Resonance (SPR) binding kinetics of IR/IRAB-A interactions and of insulin binding to IR in the absence or presence of IRAB-A. The binding results are reported in the format of k_{on} (association rate), k_{off} (dissociation rate), and K_D (binding affinity). Affinity analysis of IR/IRAB-A interactions and insulin binding to IR/IRAB-A complex was performed using a 1:1 Langmuir binding model. Affinity analysis of insulin binding to IR alone was performed using Equilibrium Steady-State model. N.D: not determined due to fast dissociation. Data reported are average of n = 2 or 3 independent experiments, except insulin binding to IR/IRAB-A complex (n = 1).

	Receptor Isoform	AVG. k_{on} (x10^5 1/Ms)	AVG. k_{off} (x 10^{-4} 1/s)	AVG. K_D (nM)
IRAB-A binding to IR	IR-A	1.04 (0.97—1.10)	2.93 (2.13—3.72)	2.82 (1.94—3.82)
	IR-B	1.00 (0.93—1.06)	2.18 (1.43—2.93)	2.18 (1.34—3.14)
Insulin binding to IR (without IRAB-A)	IR-A	N.D	N.D	>122
	IR-B	N.D	N.D	>119
Insulin binding to IR (with IRAB-A)	IR-A	4.68	7.80	1.67
	IR-B	3.09	5.49	1.78

addition, IRAB-A, in the absence of added insulin, exhibits agonist activity of IR by increasing signaling at concentrations over 3 nM.

Similar studies were repeated in the hepatocyte cell line HuH7 with endogenous IR expression. Responses in HuH7 cells were like the U2OS cells where increased IR tyrosine phosphorylation was observed as the concentration of IRAB-A increased (Figure 2C). Furthermore, IRAB-A, in the absence of added insulin, also behaved as an agonist. Kinetic analysis of IR phosphorylation over a 120 min time course revealed distinct differences in receptor activation following IRAB-A versus insulin stimulation (Figure 2D). At 1 nM, insulin alone induced a rapid increase in IR phosphorylation, peaking at approximately 5 min, while remaining elevated above baseline for the time course tested. At 30 nM, IRAB-A induced a delayed and gradual increase IR tyrosine phosphorylation. Compared to insulin, IRAB-A induced pIR stimulation achieved peak-insulin stimulated pIR levels by 10 min and continued to stimulate IR phosphorylation reaching a plateau between 30 and 120 min. We further evaluated HuH7 cells treated with IRAB-A (30 nM) for 30 min followed by insulin (1 nM). During the early phase of co-stimulation (0—10 min), pIR trends were similar to those obtained by insulin alone; at later time points (15—120 min), pIR trends resembled those of IRAB-A alone. Treatment of HuH7 cells with isotype control mAb had no effect on the kinetics of insulin stimulated pIR (Figure 2E).

To determine if IRAB-A activation of IR translated to critical downstream signaling pathways and functional endpoints, we evaluated the phosphorylation status of two critical residues on Akt, Ser473 (Figure 2F) and Thr308 (Figure 2G) [16]. IRAB-A causes a leftward shift and increased C_{max} response of the insulin dose response curves for both Akt Ser473 and Thr308 phosphorylation. We next evaluated glucose uptake in differentiated 3T3-L1 adipocytes. In the presence or absence of co-stimulatory insulin (3 nM), IRAB-A had no significant effect on 2-deoxyglucose uptake at 0.1 and 1 nM (Figure 2H). However, 10 nM IRAB-A alone increased glucose uptake by 2.0 $\pm$ 0.3-fold; the combination of IRAB-A and insulin significantly increased glucose uptake in 3T3-L1 cells over the effect of insulin alone ($P < 0.0001$).

3.3. Metabolic effects of IRAB-A in mice

3.3.1. Single dose IRAB-A causes persistent effects on glycemia in mice

Because the in vitro profile of IRAB-A was consistent with an insulin sensitizer/agonist, studies were initiated to examine the in vivo pharmacology of this unique mAb. Upon a single subcutaneous injection in lean mice, a modest acute lowering of fed blood glucose was observed (Figure 3A). This effect persisted for at least 2 weeks at the highest dose tested (25 mg/kg; Figure 3B); the duration of action was dose-dependent as the 10 mg/kg and 5 mg/kg doses showed activity for shorter periods following treatment compared to the 25 mg/kg dose. No change in body weight (BW) was observed with IRAB-A treatment (Figure 3C). To examine the pharmacodynamic/pharmacokinetic relationship between IRAB-A exposure and glucose control, a second cohort of C57 mice were administered 10 mg/kg IRAB-A or isotype control. In addition to monitoring fed blood glucose over two weeks (Figure 3D), blood samples were obtained to measure circulating insulin and human IgG1 (Figure 3E,F). Consistent with the initial finding, fed blood glucose was significantly lower in IRAB-A treated animals following a single injection, returning towards baseline at 14 days. Plasma insulin levels tracked with glycemia, whereby IRAB-A induced a reduction in circulating insulin during the first week, before returning to basal values (Figure 3E). Insulinopenic STZ-treated mice were used to show the impact of direct IR activation by IRAB-A on glycemia in vivo; a single injection of IRAB-A significantly reduced glycemia in diabetic mice for 8 days, before starting to return towards pre-treatment hyperglycemia (Suppl. Figs. S2A and B).

Detection of the administered mAb in mouse serum indicated a T_{max} of 24—72 h following injection of mAb, but the isotype control reached higher concentrations and was cleared more slowly than IRAB-A (Figure 3F). These data are consistent with specific binding of the IRAB-A to IR in peripheral tissues. To examine this more thoroughly, mice were injected with control antibody or IRAB-A, and at various timepoints over 2 weeks, tissue samples were collected and fixed for immunofluorescent detection of exogenous human IgG1. No specific staining was observed in either liver (Figure 3G) or skeletal muscle (Figure 3H) sections from mice treated with control antibody (Figure 3) or animals receiving PBS vehicle (data not shown). In contrast, IRAB-A injected mice showed specific IgG1 bound to both liver and muscle sections at 1, 3, 4 and 7 days post-treatment, but these signals were reduced on day 14. Hence, IRAB-A appears to bind to receptors in tissues relatively rapidly, and is then cleared over time. Specific insulin receptor staining in the same liver and skeletal muscle tissue sections did not show a difference in staining intensity comparing tissues from isotype control antibody injected versus IRAB-A injected mice (Supplementary Fig. S3).

3.3.2. IRAB-A alters glucose homeostasis and causes tissue specific insulin signaling changes in lean mice

Next, we evaluated the in vivo pharmacology of IRAB-A during an oral glucose tolerance test (OGTT), with parallel evaluation of insulin signaling in peripheral tissues. Normal mice were administered 10 mg/kg IRAB-A or isotype control on day 0, and given a 2 g/kg oral glucose tolerance test on day 2 following overnight fasting. Blood samples were collected for glucose, insulin, C-peptide and glucagon (Figure 4). Following the overnight fast, blood glucose levels were 116.5 $\pm$ 8.8 mg/dl in isotype control-treated mice, and IRAB-A-treated

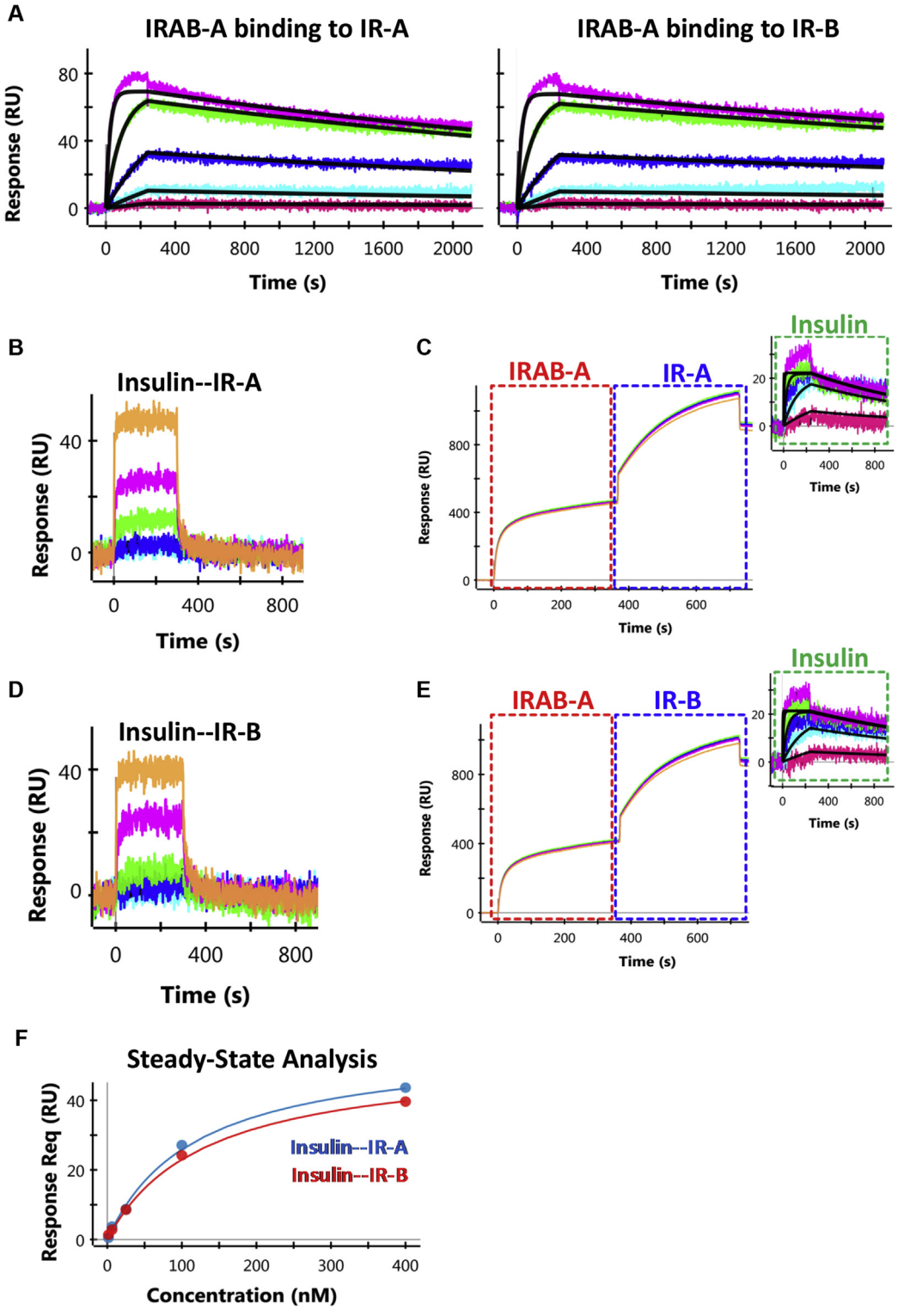

Figure 1: SPR sensorgrams for IRAB-A or insulin binding to recombinant IR. (A) High affinity binding of IRAB-A to IR-A and IR-B. IRAB-A was captured using an anti-Fc chip, followed by the titration of IR (400 nM – 1.56 nM at 4-fold dilutions). A 1:1 Langmuir model (black lines) was used to fit the binding profiles. (**B**, **D**) Weak binding of insulin to IR-A and IR-B isoforms, respectively, observed in the absence of IRAB-A. The receptors were captured through their poly-histidine tag and was followed by the titration of insulin (400 nM – 1.56 nM at 4-fold dilutions). (**C**, **E**) Insulin binding to IR-A and IR-B isoforms, respectively, measured in the presence of IRAB-A. Capture of IRAB-A is indicated by the red boxes, followed by receptor capture (blue box), and finally, the titration of insulin (2000 nM – 3.2 nM at 5-fold dilutions, green box). A 1:1 Langmuir model (black lines) was used to fit the profiles of insulin binding to the IR/IRAB-A complex. (**F**) Binding analysis of insulin binding to IR-A and IR-B using steady-state equilibrium model.

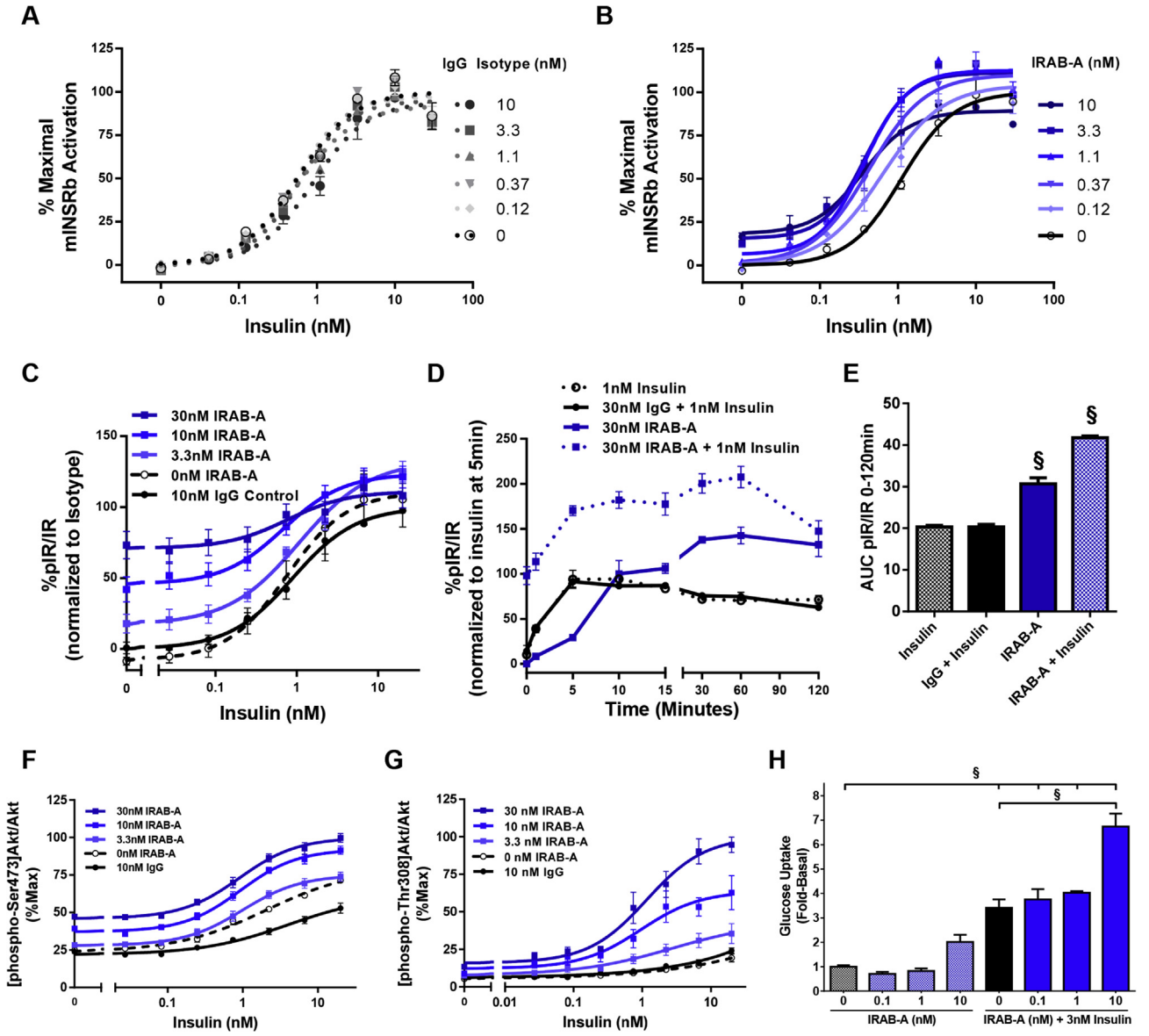

Figure 2: IRAB-A impacts IR signaling. (**A**) U2OS cells expressing the mouse IR-B isoform were treated with IgG control mAb or (**B**) IRAB-A for 30 min and then stimulated with insulin for 3 h (n = 2). (**C**) IR tyrosine phosphorylation in HuH7 treated with mAb then insulin (n = 8 except for 0 nM and Isotype where n = 4). (**D**) IR pTyr measured over a time course in HuH7 cells treated with 1 nM insulin only, 30 nM IRAB-A only or IRAB-A (isotype) followed by insulin for specified time (n = 3). (**E**) Area under the curve (AUC) for treatments in (D) is shown. (**F**) Akt Ser473 phosphorylation in HuH7 cells with 30 min mAb pretreatment and 15 min insulin dose titration (n = 8 except for 0 nM and Isotype where n = 4). (**G**) AktThr308 phosphorylation in HuH7 cells with 30 min mAb pretreatment and 15 min insulin dose titration (n = 4). (**H**) Glucose uptake in 3T3-L1 cells treated for 15 min with IRAB-A alone or IRAB-A with insulin (n = 3); N.B. control glucose uptake was reported in [14]. Concentration-response curves are graphed using Prism Graphpad software as log (agonist) vs. response, variable slope (four parameters). *P < 0.05, †P < 0.01, ‡P < 0.001, §P < 0.0001.

mice showed blood glucose levels of 46.8 ± 3.2 mg/dl (n = 8; P < 0.0001). After receiving a glucose gavage blood glucose in both treatment groups rose to a similar observed peak value at 30 min post-challenge, and returned to respective baseline fasting levels by 120 min (Figure 4A); independent replications of this study design consistently showed a similar pattern of glucose excursion in IRAB-A treated mice vs. isotype control-treated mice (data not shown). IRAB-A significantly reduced the integrated glycemic excursion (area under the curve (AUC)) in the OGTT compared to control animals (Control: 24,448 ± 786 mg/dl × 120 min vs IRAB-A: 15118 ± 1809 mg/dl × 120 min; P < 0.001). Circulating insulin and C-peptide levels showed a similar profile pattern to the glucose levels but were reduced in IRAB-A-treated mice vs. controls (Figure 4B,C) and indicate the stimulus-secretion coupling of the pancreatic beta cell is not disrupted by IRAB-A. Calculation of the HOMA-IR index using the baseline fasting blood glucose and insulin determinations made in the glucose excursion study indicated a score of 3.16 ± 0.60 for control mice, and 0.14 ± 0.03 for IRAB-A treated animals, indicative of the reduced demand for endogenous insulin. As expected, glucagon levels in IRAB-A treated animals were significantly elevated in the fasting state, and were inversely correlated with the glycemic excursion (Figure 4D). These results suggest that glucagon elevation as a normal counter-regulatory mechanism to counter hypoglycemia was intact in IRAB-A treated mice.

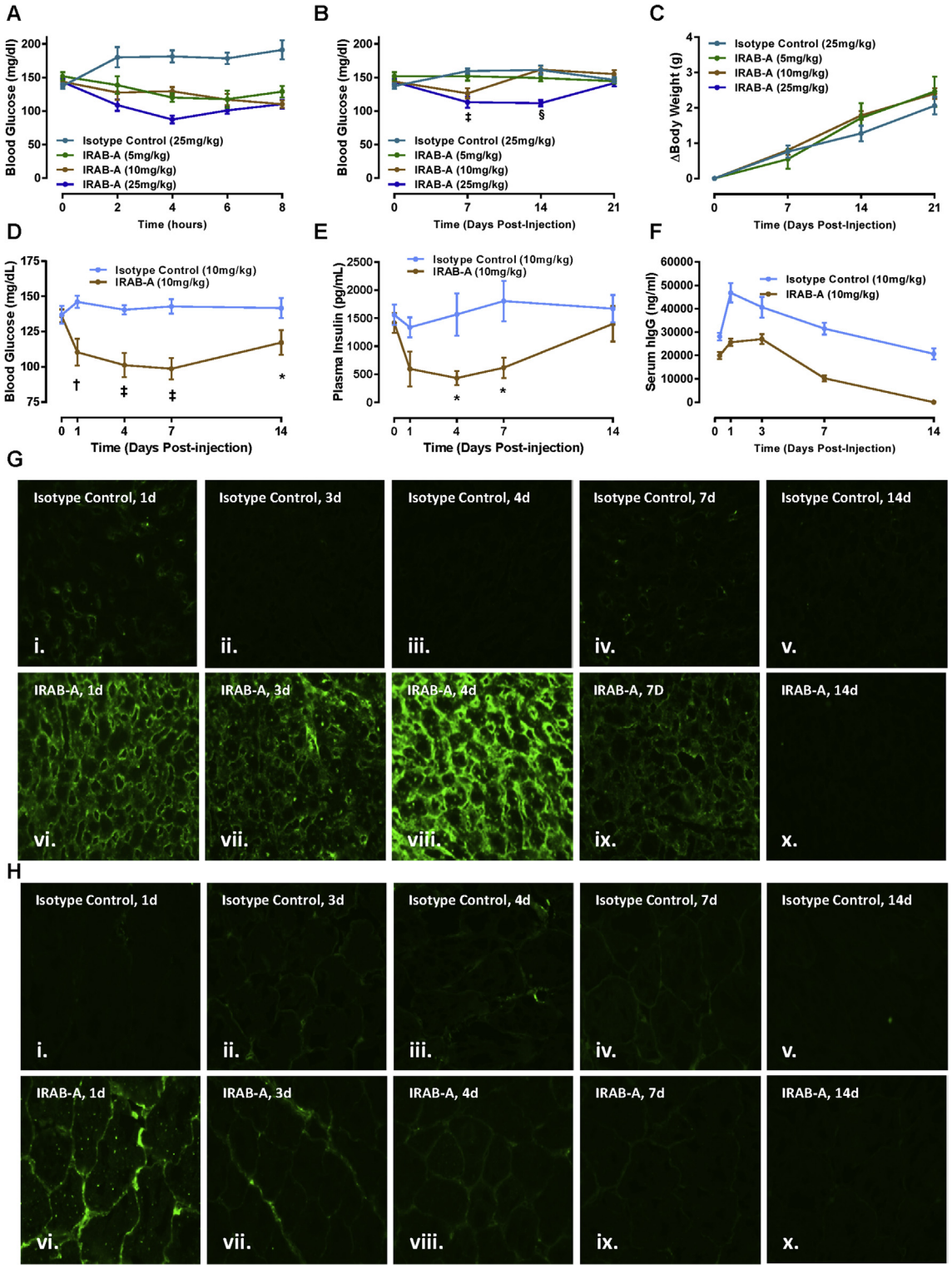

Figure 3: A single injection of IRAB-A causes persistent reduction in glycemia and insulinemia in C57Bl/6 mice over two weeks. Mice were injected subcutaneously with IRAB-A or isotype control at the indicated dosages. Fed blood glucose was acutely monitored up to 8 h (**A**), and 21 days post-treatment (**B**). (**C**) Body weight (BW) measurements were collected from animals shown in panel (**B**). (**D**) Fed blood glucose and (**E**) plasma insulin were measured in IRAB-A treated mice out to day 14 in a separate cohort of animals. (**F**) Human serum IgG was measured for both IRAB-A and Isotype control over 14 days. Data in each panel represent mean ± SEM of 8 animals; *$P < 0.05$, †$P < 0.01$, ‡$P < 0.001$, §$P < 0.0001$. (**G**) Specific human IgG tissue staining in liver and (**H**) skeletal muscle was measured in IRAB-A treated mice (vi-x) and isotype control treated animals (i–v). Images are representative of results from 3 animals per time point.

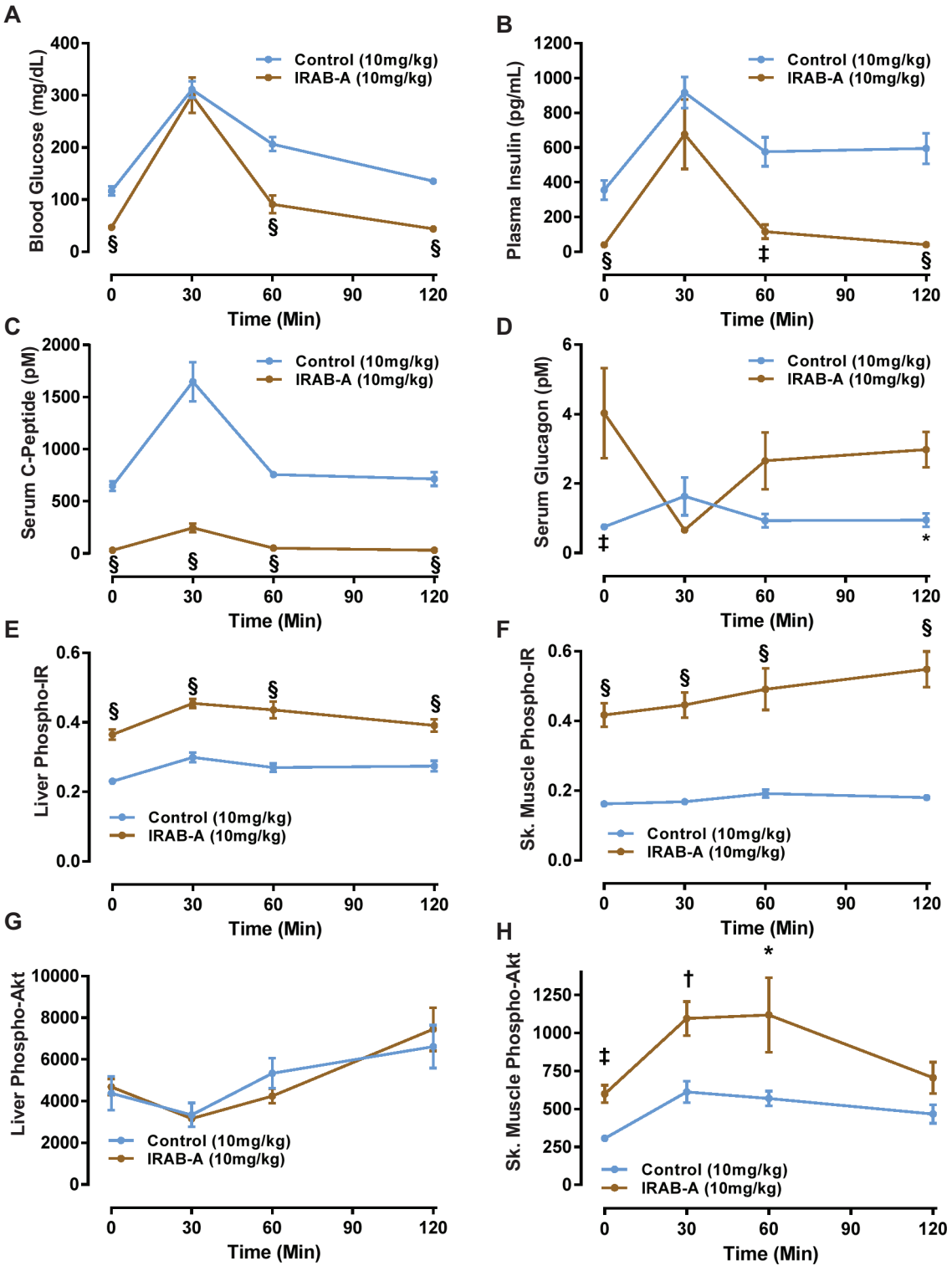

Figure 4: IRAB-A-induced changes during an oral glucose tolerance test in C57Bl/6 mice. Mice were injected with IRAB-A or isotype control (10 mg/kg) 24 h prior to an overnight fasting OGTT (2 g/kg). (**A**) Blood glucose was monitored for 120 min following the OGTT. Immunoassay of circulating (**B**) insulin, (**C**) C-peptide, and (**D**) glucagon was measured. Liver and gastrocnemius tissue extracts were analyzed at each time point for phospho-Tyr1150/1151-IR (**E** and **F**) and phospho-Ser473-Akt (**G** and **H**). Data in each panel represent mean ± SEM of 8 animals; separate cohorts of animals were tested in parallel for ex vivo tissue analysis. *P < 0.05, †P < 0.01, ‡P < 0.001, §P < 0.0001.

We collected the liver and skeletal (gastrocnemius) muscle from these mice to assess pIR and pAkt changes during the OGTT described above. At baseline (under fasting conditions), IRAB-A induced significantly elevated phospho-Tyr1150/1151-IR levels in both liver and skeletal muscle (Figure 4E,F), despite very low circulating endogenous insulin (Figure 4B). Following oral glucose administration, pIR levels were persistently elevated in IRAB-A treated mice in both peripheral tissues. However, a minor trend of increased pIR was observed in liver

extracts at 30 min in both control and IRAB-A groups, consistent with the peak stimulated endogenous insulin at this time point. Downstream insulin signaling appeared to be differentially-coupled in the two insulin target tissues we evaluated. Despite the IRAB-A stimulated increase in liver pIR levels, pAkt levels in liver were not different between control antibody and anti-IR mAb treatment groups (Figure 4G). In contrast, pAkt levels in skeletal muscle were increased by IRAB-A in the basal fasted state, and further increased in the context of the glucose excursion (Figure 4H).

3.3.3. Metabolic effects of IRAB-A in DIO mice

IRAB-A demonstrated robust pharmacology in lean mice, so we next sought to evaluate this molecule in a disease model, the DIO mouse. We created two sets of DIO mice differing in the level of insulin resistance by feeding a 60% high fat diet (HFD) for different durations. Normal mice were started on the HFD at 6 weeks of age that continued for 6 weeks to generate one cohort; or continued for 12 weeks of HFD to generate an older cohort. We anticipated that the younger cohort would show some degree of insulin resistance while the animals in the older cohort would show an even greater degree. Mice were started on HFD in a staggered fashion such that they could be tested in parallel at the target ages. The mice in the 12-week-old cohort (6 weeks of HFD) had a mean BW of 35.3 $\pm$ 0.6 g, with mean fed glycemia of 157.3 $\pm$ 5.9 mg/dl and plasma insulin levels of 1640 $\pm$ 160 pg/ml. The 18-week old cohort of DIO mice (12 weeks of HFD) were heavier (mean 46.9 $\pm$ 0.7 g with slightly higher fed glycemia (178.3 $\pm$ 6.9 mg/dl), and dramatically elevated plasma insulin (13,770 $\pm$ 3593 pg/ml) (n = 16; Figure 5A,D). These animals were then sub-divided into two cohorts and treated with IRAB-A or isotype control mAb. Twenty-four hours later blood samples were collected and results showed fed blood glucose was $\sim$17% lower in IRAB-A 12-week old DIO mice (Figure 5B), also with $\sim$20% lower circulating insulin levels; in contrast, in the older DIO mice, fed blood glucose was increased by $\sim$29% in IRAB-A treated animals versus controls, and plasma insulin was approximately 5.1-fold higher (Figure 5E). On day 2 post-injection, mice were subjected to a 6 h fast, and a mixed meal tolerance test (MMTT; 2 g/kg glucose) was performed. In both the 12- and 18-week cohorts of DIO mice, the short duration fast caused significantly greater reduction in blood glucose in the IRAB-A treated groups vs. controls, but this effect was more pronounced in the younger mice. Interestingly, fasting plasma insulin was reduced vs. controls in the younger cohort, but elevated vs. controls in the older mice (Figure 5F). The fasted blood glucose and insulin data clearly show an insulin-sensitized state in the younger DIO mice, with reduced blood glucose and reduced plasma insulin. The HOMA-IR index supported the notion of worsening insulin resistance with age (12 wk DIO Controls: 26.0 $\pm$ 3.4 vs 18 wk DIO Controls: 36.6 $\pm$ 3.0), for IRAB-A treated animals, insulin sensitization in the younger cohort (1.79 $\pm$ 0.47), but not in older mice receiving the insulin receptor mAb (41.1 $\pm$ 13.4).

The glycemic excursion observed in both 12-week and 18-week old DIO control mice administered the MMTT followed nearly identical profiles (Figure 5G,H), highlighting that although the older mice are more hyperinsulinemic, they can maintain glucose tolerance although glucose levels are elevated vs. lean mice, consistent with their degree of insulin resistance. In both cohorts of IRAB-A treated DIO mice, despite beginning with significantly lower fasting blood glucose compared to isotype-treated DIO controls, we observed diminished glucose tolerance compared to isotype control-treated mice (Figure 5G,H). Integrated glycemic excursions showed IRAB-A *increased* the blood glucose AUC by 14.1% in 12-week old DIO mice and by 56.9% in 18-week old DIO animals (Figure 5I); the impact of IRAB-A in the older DIO mice was significantly greater than in the younger, less insulin resistant mice ($P < 0.0001$). Plasma insulin samples taken at 15 min post-challenge (Suppl. Fig. S2C) paralleled baseline insulin measurements — slightly reduced insulinemia in younger IRAB-A treated mice, yet significantly elevated circulating insulin in the older cohort. In an experimental paradigm testing glucose tolerance via an intraperitoneal glucose challenge in 18-week old DIO mice — a low insulin stimulus model — IRAB-A significantly improved glucose tolerance (Suppl. Figs. S2D—F). Results from acute mouse experiments reveal a unique behavior of IRAB-A in lean mice compared to the DIO mouse model.

3.3.4. Chronic treatment of DIO mice with IRAB-A improves glycemic control in the unchallenged state

We performed multiple-dose studies in DIO mice using an IRAB-A construct, with the variable regions of IRAB-A grafted onto a murine IgG2σ Fc (mIRAB-A). First, we confirmed the activity of this construct compared to the human IgG1 version in lean C57 mice on fed blood glucose and insulinemia, as well as during an MMTT, demonstrating similar behavior (Suppl. Fig. S1). Therefore, we progressed to testing this murine IgG2σ Fc version in a multi-dose study. Fourteen-week-old DIO mice (32.4 $\pm$ 0.4 g) were dosed twice weekly with subcutaneous mIRAB-A at 3 or 10 mg/kg, or equivalent isotype control (Figure 6); this dosing paradigm achieved steady-state mAb exposure between 14 and 21 days (Suppl. Fig. S4). Multiple-dose administration of mIRAB-A at both 3 and 10 mg/kg significantly reduced fed blood glucose values compared to controls, for the duration of the 4-week study (Figure 6A). Fed plasma insulin levels were also reduced over this time span (mIRAB-A 3 or 10 mg/kg vs IgG control group, $P < 0.05$ on days 7, 14 and 24; Figure 6B). To assess the impact of chronic mIRAB-A treatment on glucose tolerance, an MMTT was performed on day 24 following a 6 h fast. Multiple-dose treatment of the IR mAb reduced 6 h fasting glycemia and insulinemia in DIO mice at 24 days (Figure 6C,D). With findings similar to those observed in the acute DIO study, multiple-dose IRAB-A treatment resulted in an exaggerated glycemic and insulin excursion relative to control-treated DIO mice (Figure 6C,D). Chronic IRAB-A appeared to cause both reduced peak insulin vs that observed in control-treated mice, but also a sustained elevated insulinemia over the course of the 2 h meal challenge; in contrast, the control group's insulin levels peaked rapidly and returned to baseline within an hour. A 1.0 U/kg intraperitoneal insulin tolerance test was performed on day 28 following a 4 h fast; baseline glycemia was significantly reduced in IRAB-A treated groups and a trend towards reduced integrated glycemia was observed (Suppl. Figs. S4A and B). Upon termination of the study (Day 30), blood chemistry analysis was performed during a partial necropsy (Suppl. Fig. S5). DIO mice treated with twice weekly doses of IRAB-A for one month had significantly reduced total cholesterol and NEFA, and a trend towards reduced plasma triglycerides.

4. DISCUSSION

This report describes the pharmacology of a novel IR mAb in cultured cells and lean and DIO mice. This antibody binds allosterically to the insulin receptor and apparently stabilizes ligand binding. IRAB-A shows both agonist and sensitizing properties and alters the kinetics and potency of insulin-induced IR activation likely due to its allosteric binding. IRAB-A substantially lowers glucose and insulin levels in lean mice for at least 14 days following a single injection. This activity is robust in lean mice but shows mixed effects on glycemia and insulinemia in obese animals depending on the length of time on DIO diet.

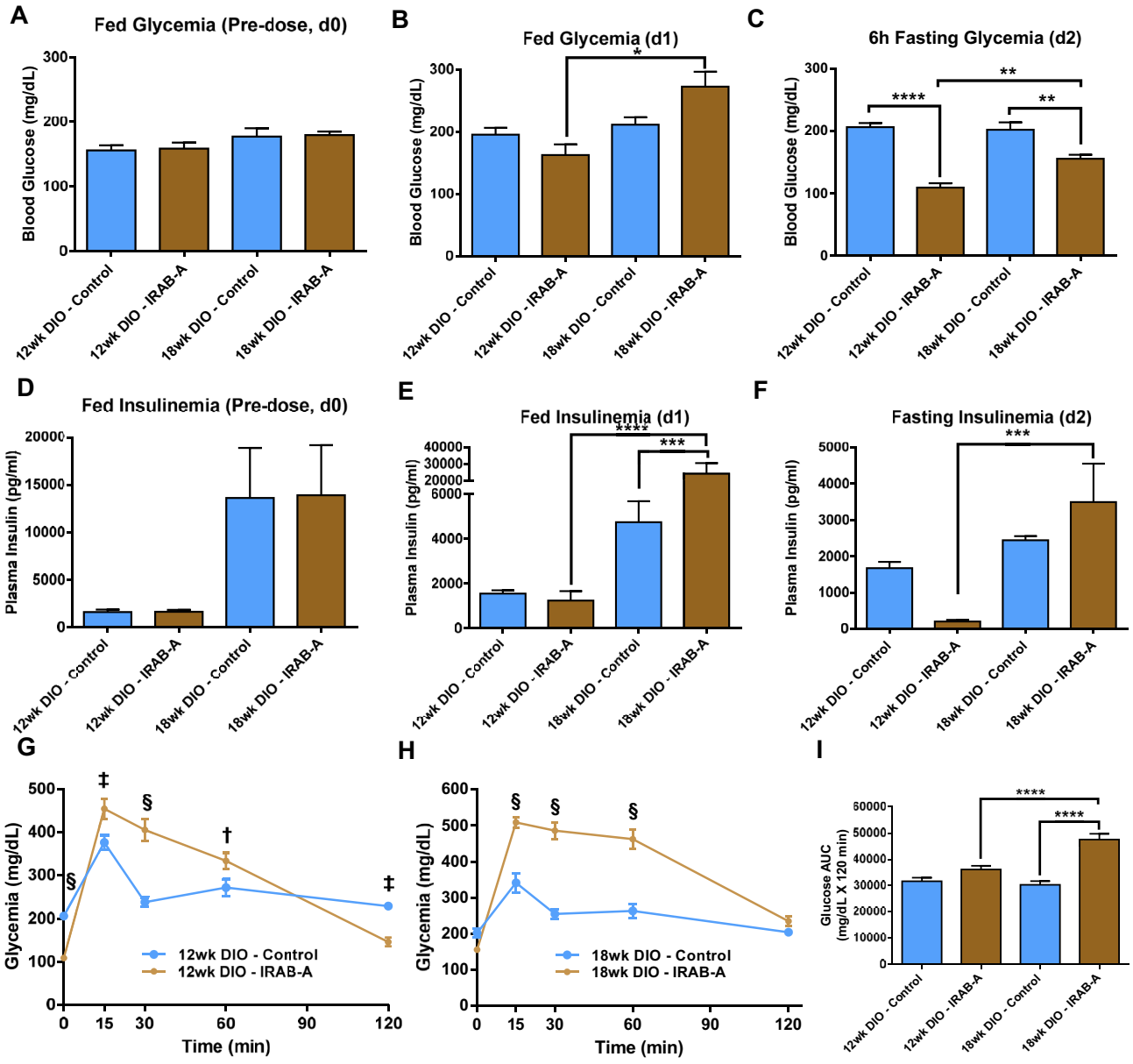

Figure 5: IRAB-A-induced metabolic changes during a mixed meal tolerance test in DIO C57Bl/6 mice. Mice were maintained on 60% high fat diet for 12 or 18 weeks to create two separate cohorts. Baseline fed blood glucose (**A**) and insulin (**D**) were measured immediately prior to antibody dosing. Animals were injected with IRAB-A or isotype control (10 mg/kg), and glucose (**B**) and insulin (**E**) were measured 24 h later. On Day 2, mice were fasted for 6 h then a mixed meal tolerance test performed; pre-challenge 6 h-fasting blood glucose and insulin was measured (**C** and **F**). Blood glucose was monitored for 120 min following the challenge in the 12 wk HFD (**G**) and 18 wk HFD mice (**H**). Integrated glycemic excursion data from G and H are plotted in panel (**I**). Data in each panel represent mean ± SEM of 8 animals. *P $<$ 0.05, †P $<$ 0.01, ‡P $<$ 0.001, §P $<$ 0.0001.

Naturally occurring IR antibodies have been identified in patients and have been reported to induce contrasting outcomes, such as insulin resistance or hypoglycemia, suggesting both inhibitory and agonistic functions [8,11–13,17–19]. These observations support that agents that modulate insulin receptor signaling in vitro may translate to robust pharmacologic effects in humans and thus support insulin receptor as a therapeutic target. One group has identified XMetD, an insulin receptor antagonist [20]. This molecule has progressed to human trials for congenital hyperinsulinemia and post-bariatric hypoglycemia. This group has also reported two positive allosteric IR mAbs: XMetA, which activates IR in the absence and presence of ligand and another antibody, and XMetS, which acts as an insulin sensitizer. Both of these antibodies both lower blood glucose levels in mice [7,21–25].

IRAB-A appears to act distinctly from previously reported antibodies. XMetA has the greatest affinity of these for the IR with a K_D of 0.04 nM while XMetS and IRAB-A have approximately equal affinities with K_D values of 3 nM [25,26]. A direct in vitro comparison is difficult as XMetA and XMetS activity was reported in an engineered CHO cell line while we analyzed IRAB-A activity in the HuH7 with endogenous IR, but there appear to be distinctions between these mAbs. In the absence of

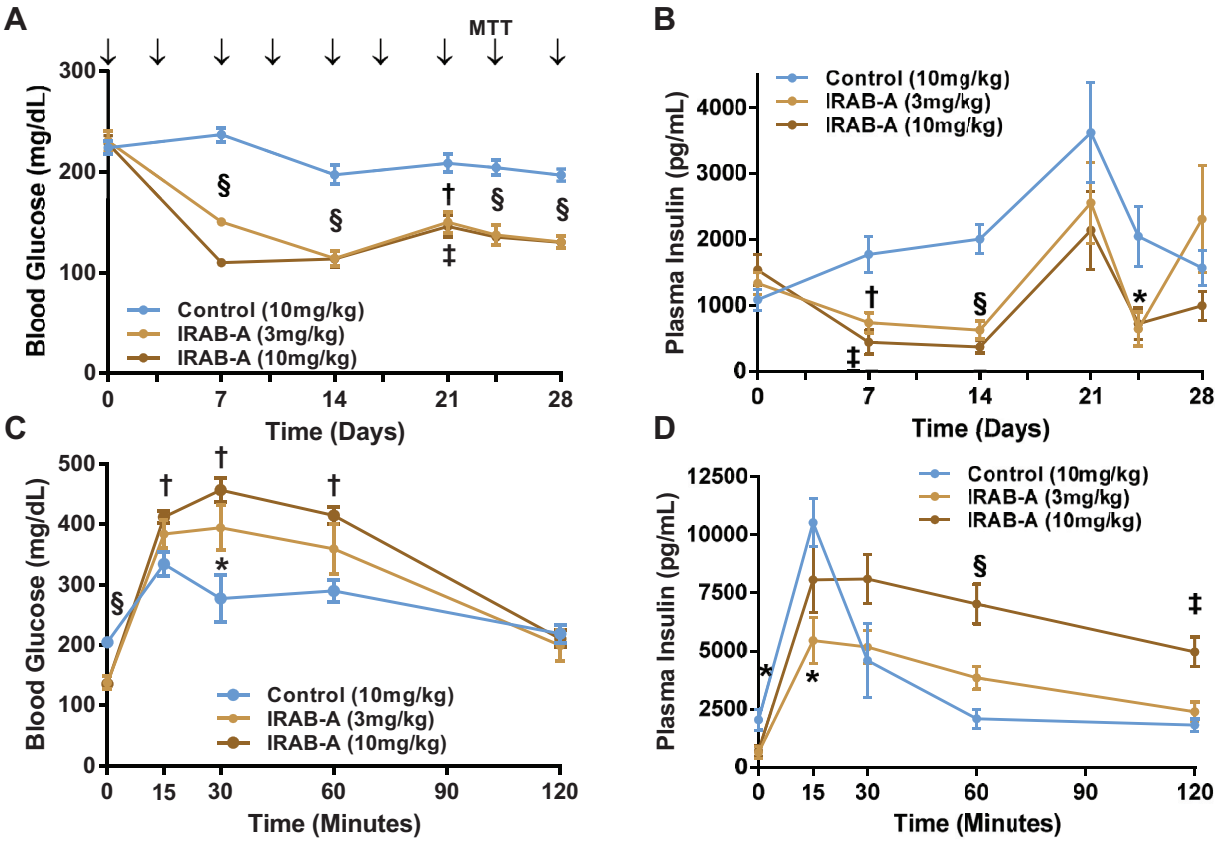

Figure 6: Chronic multiple dose IRAB-A-induced metabolic changes in DIO C57Bl/6 mice. Mice (14wks old; 8 weeks on 60%HFD at the start of the study) were injected with murine IgG2σ IRAB-A or isotype control (10 mg/kg) twice weekly for 4 weeks (indicated by arrows in panel A). (**A**) Fed blood glucose and (**B**) insulin were tracked over 28 days. On Day 24, mice were fasted for 6 h prior to a mixed meal tolerance test (with 2 g/kg glucose), and (**C**) blood glucose and (**D**) insulin measured over 120 min following the challenge. Data in each panel represent mean ± SEM of 8 animals. *P < 0.05, †P < 0.01, ‡P < 0.001, §P < 0.0001.

insulin, IRAB-A induces greater IR phosphorylation than XMetA. At 30 nM, IRAB-A alone activated the receptor to about 75% that of maximum insulin response (Figure 2C), XMetA activated IR phosphorylation to levels ~20% of maximum insulin response (Figure 2A,B) [26]. Additionally, XMetA did not appear to alter Akt C_{max} phosphorylation over an insulin dose titration whereas IRAB-A treatment led to a ~50% increase in the C_{max} of the insulin dose response curve for Akt473 phosphorylation (Figure 2) [26]. We recently reported another IR mAb, IRAB-B, that was shown to act as an effective IR antagonist [14]. Competition binding studies revealed that IRAB-B binds allosterically to the IR but at a site separate from IRAB-A (data not shown). The affinities of these molecules for the IR was approximately $K_D = 3$ nM; thus, it appears that the different pharmacological profiles of these mAbs is epitope driven, and it is possible that IRAB molecules bind at different epitopes than the three XMet antibodies.

Our in vitro experiments exhibit several critical points that demonstrate the novel pharmacology of IRAB-A distinct from insulin. IRAB-A alone activates IR signaling more slowly than ligand but induces a higher level and a longer duration of signaling. Also, co-stimulation with insulin and IRAB-A induces pIR trends that appear to be additive of both molecules and therefore appear to be independent (Figure 2D). Thus, it appears that, IRAB-A activates the receptor through its allosteric engagement and this is different from the canonical orthosteric mechanism. Furthermore, IRAB-A induces IR phosphorylation greater than ligand alone and for a longer duration (Figure 2D). Importantly, these observations are translated to the critical downstream target Akt (Figure 2F,G); thus, IRAB-A is engaging relevant signaling pathways. We hypothesize that this unique signaling profile of IRAB-A may be due to the binding kinetics of the mAb or a result of some structural changes induced by the antibody that are different from ligand. In accord with our findings, XMetA was reported to induce signaling pathway differences compared to insulin suggesting that allosteric engagement of the IR may lead to novel activation mechanisms [21]. This would need to be addressed through intensive structural studies. Our studies in lean mice demonstrated IRAB-A was effective at lowering glucose and insulin in vivo for at least 2 weeks following a single dose. Measurements of IRAB-A in serum showed that this antibody was cleared from the serum within a few days, but our IHC analyses that show that this molecule persists in at least 2 key insulin responsive tissues liver and skeletal muscle beyond 7 days (Figure 3G,H). This tissue engagement is likely responsible for the long duration of action for this antibody. We observed similar kinetics and duration of action with the antagonist molecule, IRAB-B [14].

While we observed very robust responses with IRAB-A in lean mice, activity is altered in older, insulin resistant animals, especially during an oral challenge. There may be several reasons for these observations including insulin levels, IR levels, IR signaling, change in feedback, compensatory mechanisms with older, diabetic animals. We showed signaling differences in pIR and pAkt between that of lean liver and muscle tissue; however, we predict comprehensive analysis of additional signaling targets in metabolic tissues, including adipose, from lean vs. diabetic models may offer valuable insight into these variable

physiologic responses. It is possible that these differences in IRAB-A pharmacology may point to some critical changes that occur in the pathogenesis of obesity or insulin resistance to be investigated further. Furthermore, IRAB-A may be used to provide additional physiological understanding of glucose homeostasis, such as selective insulin resistance in the diabetic liver and better define the role of the IR in metabolic complications such as NASH, T2D, insulin resistance and obesity. Thus, IRAB-A may be a useful tool in characterizing the molecular, cellular, or physiological changes that develop in the pathogenesis of metabolic disorders.

While our present work clearly demonstrates potent activity of IRAB-A, questions regarding specific engagement of IRAB-A with the IR arise from our results. It is not known at present if the mAb engages a single site on the IR or, since the IR is a preformed dimer, if a single IRAB-A molecule engages both chains of a single IR or engages adjacent IR complexes [27,28]. Engaging both binding arms simultaneously of IRAB-A raises the possibility that this contributes to the mechanism(s) of IRAB-A induced signaling. Others have reported bivalent mAb engaging and activating the erythropoietin receptor [29,30]. Engaging adjacent receptors could result in IR multimers that may have some unusual biology, which would need to be evaluated through extensive molecular or structural studies.

Taken together, this work presents a model with therapeutic potential for employing mAbs or similar biological molecules to generate unique pharmacology. Our model may also apply to other biological molecules including BiTEs, DARTs, aptamers or others. These molecules may engage orthosteric or allosteric sites and exhibit different binding kinetics to initiate novel or biased signaling events as compared to the natural ligands. One recent example was reported by Yea et al. that showed an agonist mAb induced acute myeloblastic leukemic cells into natural killer cells, a cell fate that is different from the natural ligand [31]. Currently, several mAbs that target cell surface receptors have been approved as therapeutics and many more are in clinical development [32]. It is important to note that multiple mAbs are in development for the same cellular target but these mAbs bind different epitopes. For example, BMS-663513 (Urelumab) is a CD137 agonist antibody that does not block the natural ligand binding while PF-05082599 (Utomilumab) competes with CD137 ligand binding [33,34]. Early clinical trials suggested differences in adverse reactions between these molecules [35]. While the difference in results in clinical trials can be due to a number of reasons, one clear possibility is that the epitope and impact on ligand binding may be a factor. Thus, developing mAbs for clinical applications must consider multiple factors including binding epitope and valence against the desired efficacy profile as for potential adverse events.

In summary, this study clearly demonstrates the novel pharmacology of an allosteric IR specific mAb. This molecule exhibits robust pharmacology in cultured cells where it allosterically activates the receptor with a mechanism distinct from that of the natural ligand. Additionally, this mAb increases ligand activation of the receptor to levels that exceed activity of the ligand alone in both magnitude and duration of phosphoprotein levels. This antibody also exhibits clear activity in lean mice with reductions in blood glucose and insulin levels. We show that activity changes with age and in older obese animals, induces some degree of insulin resistance. This observation may be related to the degree of obesity or insulin resistance in these animals and thus IRAB-A may be useful in studies evaluating the pathogenesis and progression of obesity or insulin resistance in animal models. Our results suggest IRAB-A may be a valuable tool for several different applications. The pharmacology of this molecule may provide some important information in structural and mechanistic studies of the IR as epitope and binding valence may provide key insights into the biology of this critical physiological hormone receptor. Finally, IRAB-A may lend therapeutic understanding into insulin sensitization strategies and drug discovery efforts for treating metabolic disorders.

AUTHOR CONTRIBUTIONS

S.A.H., A.M.C., T.K., K.D., R.N., J.A., R.P., P.C., and K.B. designed and conducted experiments. S.A.H., A.M.C., M.L.C., S.K., E.R.L., Y.L., D.L.J., J.M.W., R.B.L., and A.J.K. designed the research. S.A.H., A.M.C., J.M.W., R.B.L., and A.J.K. wrote the paper. All authors analyzed the data and contributed to manuscript preparation.

ACKNOWLEDGEMENTS

The authors would like to thank the experimental expertise of Nathaniel Wallace, Fuyong Du, John Mabus, Dave Uhlinger, Jennifer McGehee and Andrea Matter.

CONFLICT OF INTEREST

Manuscript authors are or were employees of Janssen Pharmaceutical Companies of Johnson & Johnson. Authors hold J&J company stock and may be listed as inventors on related patents derived from this work.

APPENDIX A. SUPPLEMENTARY DATA

Supplementary data related to this article can be found at https://doi.org/10.1016/j.molmet.2018.01.014.

REFERENCES

[1] Wallia, A., Molitch, M.E., 2014. Insulin therapy for type 2 diabetes mellitus. JAMA 311(22):2315–2325.

[2] Soccio, R.E., Chen, E.R., Lazar, M.A., 2014. Thiazolidinediones and the promise of insulin sensitization in type 2 diabetes. Cell Metabolism 20(4): 573–591.

[3] Salpeter, S.R., Buckley, N.S., Kahn, J.A., Salpeter, E.E., 2008. Meta-analysis: metformin treatment in persons at risk for diabetes mellitus. The American Journal of Medicine 121(2):149–157 e142.

[4] Della-Morte, D., Palmirotta, R., Rehni, A.K., Pastore, D., Capuani, B., Pacifici, F., et al., 2014. Pharmacogenomics and pharmacogenetics of thiazolidinediones: role in diabetes and cardiovascular risk factors. Pharmacogenomics 15(16):2063–2082.

[5] Consoli, A., Formoso, G., 2013. Do thiazolidinediones still have a role in treatment of type 2 diabetes mellitus? Diabetes, Obesity and Metabolism 15(11):967–977.

[6] DeFronzo, R., Fleming, G.A., Chen, K., Bicsak, T.A., 2016. Metformin-associated lactic acidosis: current perspectives on causes and risk. Metabolism 65(2):20–29.

[7] Issafras, H., Bedinger, D.H., Corbin, J.A., Goldfine, I.D., Bhaskar, V., White, M.L., et al., 2014. Selective allosteric antibodies to the insulin receptor for the treatment of hyperglycemic and hypoglycemic disorders. Journal of Diabetes Science and Technology 8(4):865–873.

[8] Chon, S., Choi, M.C., Lee, Y.J., Hwang, Y.C., Jeong, I.K., Oh, S., et al., 2011. Autoimmune hypoglycemia in a patient with characterization of insulin receptor autoantibodies. Diabetes & Metabolism J 35(1):80–85.

[9] De Pirro, R., Roth, R.A., Rossetti, L., Goldfine, I.D., 1984. Characterization of the serum from a patient with insulin resistance and hypoglycemia. Evidence for multiple populations of insulin receptor antibodies with different receptor binding and insulin-mimicking activities. Diabetes 33(3):301–304.

[10] Qing, Y., Zhou, J.G., Yuan, G., 2009. Systemic lupus erythematosus presenting as hypoglycaemia with insulin receptor antibodies and insulin autoantibodies. Lupus 18(5):457–459.
[11] Bourron, O., Caron-Debarle, M., Hie, M., Amoura, Z., Andreelli, F., Halbron, M., et al., 2014. Type B Insulin-resistance syndrome: a cause of reversible autoimmune hypoglycaemia. Lancet 384(9953):1548.
[12] Willard, D.L., Stevenson, M., Steenkamp, D., 2016. Type B insulin resistance syndrome. Current Opinion in Endocrinology Diabetes and Obesity 23(4):318–323.
[13] Yamasaki, H., Yamaguchi, Y., Fujita, N., Kato, C., Kuwahara, H., Yamauchi, M.D., et al., 2000. Anti-insulin receptor autoantibodies in a patient with type B insulin resistance and fasting hypoglycemia. Acta Diabetologica 37(4):189–196.
[14] Cieniewicz, A.M., Kirchner, T., Hinke, S.A., Nanjunda, R., D'Aquino, K., Boayke, K., et al., 2017. Novel monoclonal antibody is an allosteric insulin receptor antagonist that induces insulin resistance. Diabetes 66(1):206–217.
[15] Baker, A.E., Mantz, A.R., Chiu, M.L., 2014. Raman spectroscopy characterization of antibody phases in serum. MAbs 6(6):1509–1517.
[16] Manning, B.D., Toker, A., 2017. AKT/PKB signaling: navigating the network. Cell 169(3):381–405.
[17] Kim, S.W., Won, H.K., Seok, H., Lee, B.W., Jung, C.H., Lee, W.J., et al., 2012. High prevalence of both anti-insulin and anti-insulin receptor antibodies in Korean patients with insulin autoimmune syndrome. Diabetes Research and Clinical Practice 98(2):e12–15.
[18] Rodriguez, O., Collier, E., Arakaki, R., Gorden, P., 1992. Characterization of purified autoantibodies to the insulin receptor from six patients with type B insulin resistance. Metabolism 41(3):325–331.
[19] Sahin, M., Tutuncu, N., Guvener, N.D., 2004. Autoimmune hypoglycemia in a type 2 diabetic patient with anti-insulin and insulin receptor antibodies. Diabetes Care 27(5):1246–1247 author reply 1247.
[20] Corbin, J.A., Bhaskar, V., Goldfine, I.D., Issafras, H., Bedinger, D.H., Lau, A., et al., 2014. Inhibition of insulin receptor function by a human, allosteric monoclonal antibody: a potential new approach for the treatment of hyperinsulinemic hypoglycemia. MAbs 6(1):262–272.
[21] Bedinger, D.H., Goldfine, I.D., Corbin, J.A., Roell, M.K., Adams, S.H., 2015. Differential pathway coupling of the activated insulin receptor drives signaling selectivity by XMetA, an allosteric partial agonist antibody. Journal of Pharmacology and Experimental Therapeutics 353(1):35–43.
[22] Bedinger, D.H., Kieffer, D.A., Goldfine, I.D., Roell, M.K., Adams, S.H., 2015. Acute treatment with XMetA activates hepatic insulin receptors and lowers blood glucose in normal mice. Journal of Cellular Biochemistry 116(9):2109–2119.
[23] Bezwada, P., Zhao, J., Der, K., Shimizu, B., Cao, L., Ahene, A., et al., 2016. A novel allosteric insulin receptor-activating antibody reduces hyperglycemia without hypoglycemia in diabetic cynomolgus monkeys. Journal of Pharmacology and Experimental Therapeutics 356(2):466–473.
[24] Bhaskar, V., Lau, A., Goldfine, I.D., Narasimha, A.J., Gross, L.M., Wong, S., et al., 2013. XMetA, an allosteric monoclonal antibody to the insulin receptor, improves glycaemic control in mice with diet-induced obesity. Diabetes, Obesity and Metabolism 15(3):272–275.
[25] Corbin, J.A., Bhaskar, V., Goldfine, I.D., Bedinger, D.H., Lau, A., Michelson, K., et al., 2014. Improved glucose metabolism in vitro and in vivo by an allosteric monoclonal antibody that increases insulin receptor binding affinity. PLoS One 9(2):e88684.
[26] Bhaskar, V., Goldfine, I.D., Bedinger, D.H., Lau, A., Kuan, H.F., Gross, L.M., et al., 2012. A fully human, allosteric monoclonal antibody that activates the insulin receptor and improves glycemic control. Diabetes 61(5):1263–1271.
[27] Belfiore, A., Frasca, F., Pandini, G., Sciacca, L., Vigneri, R., 2009. Insulin receptor isoforms and insulin receptor/insulin-like growth factor receptor hybrids in physiology and disease. Endocrine Reviews 30(6):586–623.
[28] Hubbard, S.R., 2013. The insulin receptor: both a prototypical and atypical receptor tyrosine kinase. Cold Spring Harbor Perspectives in Biology 5(3):a008946.
[29] Elliott, S., Lorenzini, T., Yanagihara, D., Chang, D., Elliott, G., 1996. Activation of the erythropoietin (EPO) receptor by bivalent anti-EPO receptor antibodies. Journal of Biological Chemistry 271(40):24691–24697.
[30] Schneider, H., Chaovapong, W., Matthews, D.J., Karkaria, C., Cass, R.T., Zhan, H., et al., 1997. Homodimerization of erythropoietin receptor by a bivalent monoclonal antibody triggers cell proliferation and differentiation of erythroid precursors. Blood 89(2):473–482.
[31] Yea, K., Zhang, H., Xie, J., Jones, T.M., Lin, C.W., Francesconi, W., et al., 2015. Agonist antibody that induces human malignant cells to kill one another. Proceedings of the National Academy of Sciences of the United States of America 112(45):E6158–E6165.
[32] Dempke, W.C.M., Fenchel, K., Uciechowski, P., Dale, S.P., 2017. Second- and third-generation drugs for immuno-oncology treatment-The more the better? European Journal of Cancer 74:55–72.
[33] Ascierto, P.A., Simeone, E., Sznol, M., Fu, Y.X., Melero, I., 2010. Clinical experiences with anti-CD137 and anti-PD1 therapeutic antibodies. Seminars in Oncology 37(5):508–516.
[34] Fisher, T.S., Kamperschroer, C., Oliphant, T., Love, V.A., Lira, P.D., Doyonnas, R., et al., 2012. Targeting of 4-1BB by monoclonal antibody PF-05082566 enhances T-cell function and promotes anti-tumor activity. Cancer Immunology Immunotherapy 61(10):1721–1733.
[35] Yonezawa, A., Dutt, S., Chester, C., Kim, J., Kohrt, H.E., 2015. Boosting cancer immunotherapy with anti-CD137 antibody therapy. Clinical Cancer Research 21(14):3113–3120.

